Earth Systems, Resources, and Sustainability, 2026, 1(2), 129–142

Scilight

Earth Systems, Resources, and Sustainability

Journal Homepage: https://www.sciltp.com/journals/esrs

Article

Boiling, Degassing, and Mixing of Fluids in the Trans-Himalayan Geothermal Systems, India

Archisman Dutta[1,2,*], Sitangshu Chatterjee[3], Parashar Mishra[4], Ashok Singh[1], Anubha Bhandari[1,*], Muduru Lachhana Dora[5], Pramod Kumar Singh[6], Biswajit Ray[2] and Vivek Prakash Malviya[7]

[1] Geological Survey of India, Northern Region, Lucknow 226024, India
[2] Department of Chemistry, Institute of Science, Banaras Hindu University, Varanasi 221005, India
[3] Isotope Hydrology Section, Isotope and Radiation Application Division, Bhabha Atomic Research Centre (BARC), Mumbai 400085, India
[4] Geological Survey of India, State Unit Jammu J&K UT Ladakh, NR, Jammu 180006, India
[5] School of Environmental Sciences, Jawaharlal Nehru University, New Delhi 110067, India
[6] Geological Survey of India, Central Headquarters, Kolkata 700016, India
[7] Department of Applied Geology, Dr. Harisingh Gour Vishwavidyalaya, Sagar 470003, India
[*] Correspondence: duttaarchisman1@gmail.com (A.D.), ab.anubhabhandari@gmail.com (A.B.)

ABSTRACT

Geothermal fluids, during ascent, are subjected to various secondary processes which alter their chemistry from reservoir to surface discharge. We have characterized and quantified various secondary processes such as degassing, boiling, and mixing in this study for the Trans-Himalayan geothermal fluids. The geochemical facies of thermal waters are found to be Na–Cl for Puga, mixed type (Na–Cl–SO_4–HCO_3) for Chumathang and Panamik, and Na–HCO_3 type for Changlung having neutral to moderately alkaline pH (6.7–8.9) along with TDS ranging from 525 mg/l to 2931 mg/l. The geothermal reservoir temperature calculated from the Na–K cation geothermometry varies between 170–260 °C. The reservoir fluids, constructed by adding liquid and steam phases compositions, exhibit near-neutral pH (6.47–7.03) with lower TDS than surface discharges (∼561–1811 mg/l). The surface geothermal water is found to be the resultant mixture of three end-members (non-thermal water, boiled reservoir water, and condensed steam) based on which a ternary mixing model has been developed. The SiO_2–temperature relation indicates undersaturation with respect to amorphous silica but equilibrium to supersaturation with respect to chalcedony and quartz. This pattern implies boiling-driven fluid evolution, kinetically controlled silica scaling, and progressively more mature reservoir waters from Panamik and Puga geothermal area. Geochemical modeling result shows that all geothermal fluids have >40% of boiled deep fluids, traced with conservative component, Cl. The fraction of condensed steam is highest in Changlung (∼11–34%) and lowest in Chumathang (∼13%) and Panamik (∼2–19%) with Puga lying in the intermediate stage (∼8–24%) (traced with reactive component, dissolved CO_2). All thermal waters exhibit mixing with local meteoric waters, with cold-water contributions ranging from 14–42%. Overall, these results highlight the role of boiling and mixing phenomenon shaping the fluid composition of the Trans-Himalayan geothermal systems.

ARTICLE INFO

History:

Received 15 December 2025
Revised 15 January 2026
Accepted 22 January 2026
Published: 29 January 2026

Keywords:

decompression boiling; secondary processes; deep fluid reconstruction; end-members fluid compositions

Citation:

Dutta, A.; Chatterjee, S.; Mishra, P.; et al. Boiling, Degassing, and Mixing of Fluids in the Trans-Himalayan Geothermal Systems, India. *Earth Systems, Resources, and Sustainability* **2026**, *1*(2), 129–142. https://doi.org/10.53941/esrs.2026.100009

Research Highlights

- Characterizing degassing, boiling, and mixing in the Trans-Himalayan geothermal fluids.
- The surface geothermal water is a mixture of three end-members (non-thermal water, boiled reservoir water, and condensed steam).
- Geochemical modeling shows that all geothermal fluids have >40% of boiled deep fluids.
- Results highlight the role of boiling and mixing that shaped the fluid composition of the Trans-Himalayan geothermal systems.

1. Introduction

Geothermal systems in active orogenic regions represent significant natural heat and fluid reservoirs and are characterized by complex hydrothermal processes such as high-temperature water–rock interaction, boiling, degassing, phase separation, magmatic or metamorphic gas influx, and mixing with shallow groundwater [1–4]. The chemical and isotopic compositions of thermal fluids preserve integrated signatures of these subsurface processes, making them valuable indicators of reservoir evolution [5, 6]. Quantifying such subsurface fluid dynamics is therefore crucial for understanding the physical and chemical evolution of geothermal reservoirs, assessing their resource potential, and deciphering the tectono-magmatic framework in which they operate [7–10].

The Trans-Himalayan region of India, located in the Ladakh Himalayas, hosts several medium- to high-enthalpy geothermal systems like Puga, Chumathang, Changlung, and Panamik, which are aligned along major crustal discontinuities such as the Main Central Thrust (MCT), Indus-Tsangpo Suture Zone (ITSZ), and Shyok Suture Zone (SSZ). These geothermal provinces exhibit anomalously high heat-flux values (>468 mW/m^2) and exceptionally steep geothermal gradients (>100 °C/km), and host numerous hot springs with surface temperatures of 60–90 °C [11, 12]. The waters show diverse geochemical facies, ranging from Na–Cl-rich mature fluids to dilute mixed-type compositions [13]. Previous studies have highlighted the influence of deep metamorphic CO_2 influx, enrichment of critical elements (e.g., Li, Cs, B, W), and near-surface mineral precipitation in shaping the chemistry of these waters [7, 14–18]. However, most earlier investigations focused on surface geochemistry, major-ion distributions, or silica geothermometry, often without correcting for steam loss or volatile partitioning [18]. As a result, the magnitude of deep-seated processes, such as adiabatic boiling, partial-equilibrium degassing, and mixing with non-thermal waters, etc. remains poorly constrained across the Trans-Himalayan geothermal provinces. In contrast, comparable systems in Iceland, El Salvador, and Kenya have been extensively modeled to delineate fluid pathways, reservoir conditions, and energy potential [2, 6, 19, 20]. Integrated applications of stable O–H and Sr isotopes, constrained by binary mixing models between non-thermal meteoric water and deep magmatic–hydrothermal end-members, have been successfully employed to quantify fluid mixing processes in geothermal systems such as the Yangbajing geothermal field on the Tibetan Plateau [21, 22]. However, a similar quantitative treatment is lacking for the Trans-Himalayan geothermal systems in India.

A key challenge in Himalayan geothermal studies is that surface waters rarely represent pristine reservoir compositions. During ascent, geothermal fluids undergo depressurization boiling, degassing of volatiles (CO_2, H_2S, Non-condensable gases or NCGs like He, H_2, Ar, N_2), silica re-equilibration, and variable mixing with shallow meteoric waters [23]. These processes modify pH, salinity, redox conditions, and reactive-solute inventories, thereby complicating conventional geothermometry and geochemical facies interpretation [24]. Multi-component geochemical modelling tools, such as WATCH and PHREEQC, offer robust frameworks to address these challenges by reconstructing deep reservoir fluid compositions, quantifying steam–liquid separation processes, and evaluating mineral–fluid equilibria under evolving thermodynamic conditions [2, 4–6, 17]. In this context, a three-end-member mixing model, comprising of boiled reservoir water, condensed steam, and non-thermal waters, is applied to quantify mixing ratios and to assess the dominant secondary processes controlling surface water chemistry. This approach has been successfully implemented in Icelandic geothermal systems and is broadly applicable to surface geothermal settings, provided that the chemical compositions of the end members are well constrained [20].

In this study, we have used such ternary mixing model approach, developed by [20] for Icelandic geothermal waters based on various end-members compositions, assuming that surface discharge is a resultant of condensed steam, non-thermal water and boiled deep reservoir water, to quantitatively constrain multiple secondary processes reservoir like boiling, degassing, and mixing for four major Trans-Himalayan geothermal systems in India. Using WATCH speciation modeling, we reconstruct deep reservoir water compositions by adding steam and liquid phases compositions and by simulating adiabatic decompression boiling under partial-equilibrium degassing (ξ = 0.5). These reconstructed fluids are subsequently used to assess various subsurface phenomena such as mixing, phase segregation, solute redistribution between liquid and steam phases, and mineral-fluid equilibria.

2. Geological Outlines of the Study Area

The Trans-Himalayan sector of Ladakh represents the former active continental margin of the Eurasian Plate that evolved during the northward subduction and eventual closure of the Neo-Tethys Ocean [25, 26] (Figure 1). To the southeast, the Tso Morari Complex comprises Proterozoic to Palaeozoic quartzo-feldspathic gneisses and metasedimentary sequences, including high-pressure–ultrahigh-pressure assemblages that document deep subduction of continental crust during the India–Eurasia convergence [27, 28]. Overlying this basement, the Rupshu Group includes Palaeozoic–Mesozoic carbonates, quartzites, and shale formations that collectively record the passive-margin evolution of the northern Indian plate [29].

The Indus Suture Zone (ISZ) in central Ladakh is represented principally by the Sangeluma Group and the Indus Group, both of which preserve the remnants of oceanic lithosphere and volcanic-arc sedimentation prior to collision [30, 31]. The Sangeluma Group consists of a dismembered ophiolite suite-serpentinized harzburgite, dunite, layered and isotropic gabbro, and pillow basalts, interpreted as fragments of Neo-Tethyan oceanic lithosphere accreted during subduction [32, 33]. East of these ophiolites, the Indus Group forms a folded and thrusted volcano-sedimentary succession tectonically emplaced over the Sangeluma units, reflecting sedimentation within arc to back-arc basins prior to the final India–Eurasia continental collision [34, 35]. A major linear intrusive complex, the Ladakh batholith is situated between the ISZ to the south and the Shyok Suture Zone to the north. The batholith comprises diverse intrusive lithologies including granite, granodiorite, tonalite, diorite, gabbro, aplite, and pegmatite along with associated volcanic and mantle-derived rocks that record multiphase magmatism associated with continental-arc activity during the Cretaceous-Paleogene closure of the Neo-Tethys [28, 34]. Extending for several hundred kilometres along the Indus Valley, this batholith forms the backbone of the Trans-Himalayan continental-arc system.

North of the batholith lies the Karakoram Batholith, separated by the Shyok Suture Zone, a tectonic belt containing oceanic remnants such as volcanics, pelagic sediments, and mélange units that mark an earlier subduction-accretion system [36]. The Karakoram Batholith is a long-lived intrusive complex comprising granites, granodiorites, monzonites, tonalites, and high-grade metamorphic basement rocks with crystallization ages ranging from the Jurassic to Miocene, reflecting repeated pulses of magmatism along the southern Eurasian margin [37, 38]. It is cut by major shear zones, most prominently the Karakoram Fault that enhance crustal permeability and influence regional geothermal gradients [36, 39].

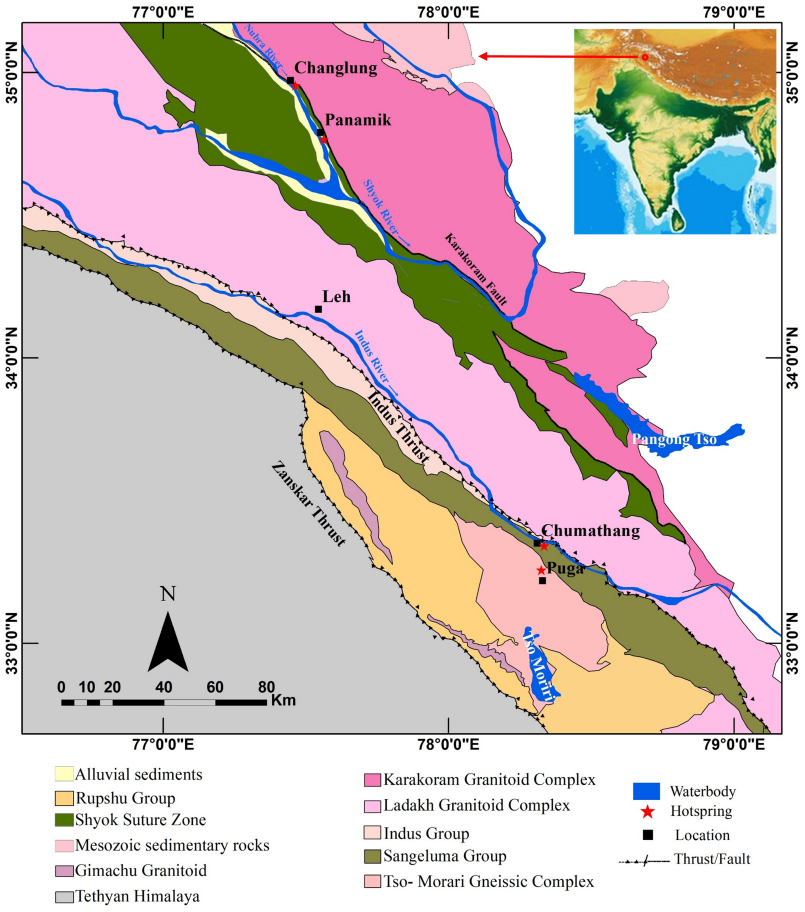

Figure 1. Geological map showing the location of hot springs (sampling sites) of Ladakh Union Territory, India (Modified after [40]).

3. Methods

3.1. Sampling and Chemical Analyses

A total of 30 thermal water samples were collected from geothermal sites in the Indus River Valley and the Shyok–Nubra River Valley and analysed [7, 41]. Of these, 18 samples were obtained from the Puga and Chumathang geothermal systems in the Indus River Valley which are collected from hot spring discharges, steam vents, and boreholes. A total of 12 samples were collected from thermal springs of Changlung–Panamik geothermal system in the Shyok River Valley. In addition, one representative non-thermal water sample was also collected for comparison. The physicochemical parameters like pH, electrical conductivity (EC), redox potential (E_H), temperature, resistivity, salinity, and dissolved oxygen were measured onsite using Hanna 9829 Multiparameter Water Quality Portable Meter. The total dissolved CO_2 (alkalinity), hardness, calcium, and magnesium were estimated onsite through titration techniques [42]. All titrations were performed in triplicate in the field to ensure analytical repeatability and accuracy [43]. Water samples were filtered with 0.2 µm cellulose acetate filter paper and collected in two batches using high-density polypropylene (HDPE) bottles: (i) a 500 ml bottle for the analysis of major cations and anions (unpreserved and unacidified); (ii) a 60 ml bottle diluted 1:10 with deionized water for silica analysis [44, 45].

Major cations, Na and K, were analysed in the Systronics 128 flame photometer; Cl is estimated by argentometric titration; UV–VIS spectrophotometer (Systronics) was used for sulfate and silica. Boron was estimated using D-mannitol titration method with NaOH [44] and fluoride was estimated through Horiba made ion selective electrode. The analytical precision based on replicate analyses of chemical parameters and inorganic charge balance error lies within ±5% at 95% confidence level. Gas or steam sampling was done in pre-evacuated 125 ml gas-bulbs and Tedlar bags. All the non-condensable gases (Ar, O_2, N_2, CH_4, H_2, and He) and condensable gases (CO_2 and H_2S) are analysed in Varian 450 GC gas chromatograph instrument.

3.2. Geochemical Modelling

In the present study, three distinct sets of geochemical calculations are done in WATCH speciation program [2, 46, 47].

Firstly, the geochemical modelling of thermal fluids is done by incorporating average liquid and steam phases compositions of four different geothermal sites to produce WATCH input file (Figure 2). This process is done by involving correction of the dissolved solids content and pH of the water phase taking steam loss into account and adding the gases that degassed upon boiling back into the liquid phase. Now, deep fluid composition is estimated for all the geothermal sites using Na–K Giggenbach's geothermometer [48]. Secondly, the same WATCH input file is again run by theoretically assuming a liquid-only single-phase reservoir ($X_{RES}^{Steam} = 0$) and thermal fluids are allowed to boil through decompression from arbitrary temperature of 300 °C to 100 °C (boiling point of pure water at NTP) in six steps which takes into account continuous phase segregation. Such assumption makes the reservoir to behave like a closed system in which the boiling is considered to be adiabatic, and degassing is assumed to be partial (degassing coefficient, $\xi = 0.5$). The depressurization boiling process induces cooling and phase segregation processes where volatiles (CO_2, H_2S, and other NCGs) accumulate in steam phase and non-volatiles (Na, K, Cl, etc., along with dissolved CGs) enrich in liquid phase. Such process affects reservoir pH, total solute content, and fluid-mineral equilibria in resultant geothermal water.

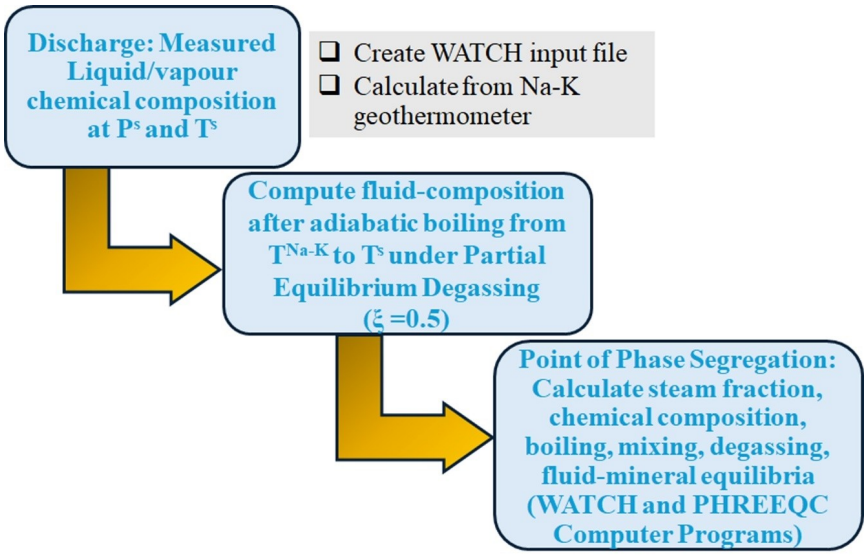

Figure 2. Flow diagram depicting deep fluid composition computation in WATCH speciation program [46] and fluid-mineral equilibria studies in PHREEQC program [47] done in the present study.

Now, based on the conservation of enthalpy and mass, we calculate the steam fraction from following equations, where H_{RES}, H_{Steam}, and H_{Liquid} are the enthalpies of reservoir fluid, steam and discharging liquid phases, respectively, and X^{steam} is the corresponding steam fraction (Equations (1) and (2)):

$$H_{RES} = X^{steam} H_{Steam} + \left(1 - X^{steam}\right) H_{Liquid} \quad (1)$$

$$X^{steam} = \frac{H_{RES} - H_{Liquid}}{H_{Steam} - H_{Liquid}} \quad (2)$$

The enthalpy of saturated-steam is sum of the steam-saturated enthalpy of liquid phase and latent heat of vaporization, all of the values of which can be derived from Steam Tables. The deep fluid composition and intermittent fluid composition during upwelling of fluids through depressurization after adiabatic boiling is estimated using the following equation, where $C_{j,\,RES}$, $C_{j,\,Steam}$ and $C_{j,\,Liquid}$ are the composition of jth-component in deep reservoir, steam and liquid phases, respectively (Equation (3)):

$$C_{j,\,RES} = X^{Steam} C_{j,\,Steam} + \left(1 - X^{Steam}\right) C_{j,\,Liquid} \quad (3)$$

Thirdly, as Cl is a conservative component, a geochemical model is developed based on conservation of enthalpy and non-reactivity of Cl upon mixing to delineate mixing fractions through varying end-member compositions. The three different end-members were chosen for such computation which are boiled reservoir water at 100 °C, gas or steam composition (consisting only volatiles), and non-thermal water (prima facie for mixing). Obtaining the information of various secondary processes, the resultant fluid composition will be used as an input file for PHREEQC program to estimate the roles of these end-members in controlling surface fluid chemistry at discharge temperatures and fluid-mineral equilibria using Lawrence Livermore National Laboratory (LLNL) thermodynamic database [47].

4. Results

The sampled thermal waters of Trans-Himalayas have discharge temperatures of 61–87 °C; pH of the solution is nearly neutral to moderately alkaline, varying between 6.7–8.9 with total dissolved solids (TDS) of 525–2931 mg/l. The reduction potential of these waters ranges between −526 mV to −397 mV. The elemental composition of the sampled thermal waters is given in Table S1 of the electronic supplementary information (ESI) file. The concentrations of major condensable gas like CO_2 are 28.1–118.7 mmol/kg, 32.2–312.4 mmol/kg, 182.4 mmol/kg, and 103.9–275.3 mmol/kg for Chumathang, Puga, Panamik, and Changlung, respectively. The concentration of other condensable gas, i.e. H_2S lies between 2.6–22 mmol/kg for all the geothermal fields (Table S2 of ESI). Based on major element composition, major geochemical facies of thermal waters are found to be Na–Cl for Puga, mixed type (Na–Cl–SO_4–HCO_3) for Chumathang and Panamik, and Na–HCO_3 type for Changlung, as illustrated in Piper diagram (Figure 3). Puga springs show the highest total ion budget with TDS ∼ 2400–2900 mg/l, dominated by elevated Na, K, Cl, and SO_4, with consistently high SiO_2 (150–232 mg/L) and boron (mean value 124 mg/l). Chumathang waters have moderate TDS (1150–1700 mg/L) with comparatively lower Cl than Puga and higher SO_4 (182–201 mg/l), with substantial silica (105–220 mg/l). Mg content is found to be higher in Chumathang thermal fluids than Puga, suggesting probably greater extent of dilution by the Indus River [49, 50]. The Changlung thermal waters are characterized by very high total dissolved inorganic carbon with values ranging between 1574–1821 mg/l, with moderate values of Cl and SO_4 concentrations. These waters have high Na and relatively low Ca–Mg, indicating a mature, chloride-rich geothermal system. In contrast, Panamik waters are the least mineralized (TDS ∼ 520–620 mg/L), with low Na, K, Cl, and silica, reflecting cooler and more dilute fluid compositions. Overall, the ion distributions show a general dominance of Na–Cl–SO_4 types across the fields, with silica decreasing from Puga/Chumathang towards Panamik.

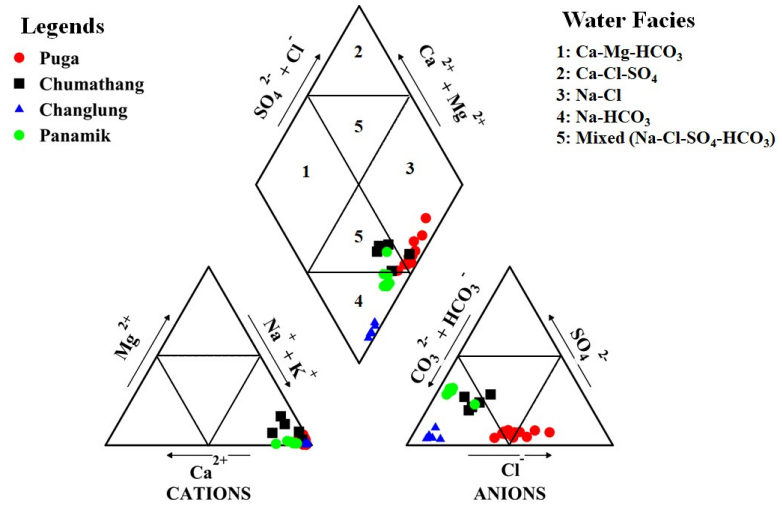

Figure 3. Piper diagram representing geochemical facies of thermal waters in Trans-Himalayas, India.

The slight divergence in trends between the Puga and Changlung samples in the Piper diagram reflects differences in secondary hydrogeochemical processes acting during fluid ascent, rather than fundamentally different deep reservoir sources. Puga thermal waters plot closer to the Na–Cl/mixed Na–Cl–SO_4–HCO_3 facies, indicating a stronger influence of deep reservoir fluids, with comparatively limited dilution. Their chemistry is mainly controlled by water–rock interaction at depth, ion exchange, and partial boiling [7, 14–16]. While Changlung samples, in contrast, shift toward the Na–HCO_3 facies, suggesting a greater role of shallow processes, such as mixing with meteoric or non-thermal groundwater, CO_2-reabsorption at shallower levels, and near-surface re-equilibration. Thus, the observed variation arises from different degrees of mixing, dilution, and re-equilibration along distinct flow paths, controlled by local structural permeability and hydrological conditions, even though both systems may ultimately derive heat from a similar regional geothermal regime [49–51].

5. Discussions

5.1. Geochemical Evolution of Solutes

The Puga and Chumathang geothermal sites comprise of boiling springs (biphasic: both steam and liquid) along with geyseric manifestation and high discharge rates. In Puga, the total natural discharge reaches nearly 30 L/s (about 108 tons/hour). Such a high outflow suggests limited opportunity for near-surface re-equilibration or silica loss through shallow mixing with non-thermal waters [52]. Thermal waters of Puga are dilute Cl–HCO_3 type (as per Cl–SO_4–$\sum CO_2$ ternary diagram) and Chumathang are dilute Cl–HCO_3–SO_4 type (mixed-type), where sulfate enrichment may have happened due to oxidation of past fumarolic sulfur deposits (Figure 4a). Lower Cl content and moderate TDS, unlike Puga, also indicate greater lateral flow for Chumathang fluids than Puga fluids [7]. Recent studies have shown the signature of thenardite, epidote, polylithionite, lepidolite, zinnwaldite, jarosite-K, and alunite are observed from powder X-ray diffraction studies of hot spring deposits [16, 53–58]. The occurrence of epidote as hydrothermal mineral deposit is an indication of subsurface temperature of 250 °C while thenardite is a paleo-humidity indicator mineral suggesting a humidity-transit past climatic conditions and jarosite-K occurrence suggests an early Martian type climate conditions in the past [16, 54–58].

As per Figure 4a, Changlung thermal waters are HCO_3-dominated while Panamik fluids are dilute Cl–HCO_3–SO_4 type (mixed-type geochemical facies), like Chumathang. In Changlung, enhanced HCO_3 could be due to reabsorption of deep-degassed CO_2 at near surface, after steam segregation (predominantly continuous over single-stage) from deeper levels in thermal waters mainly due to decompression boiling of fluids. The CO_2 present in the Changlung thermal waters may originate from either metamorphic or magmatic sources, and the measured $\delta^{13}C$–$\sum CO_2$ (dissolved inorganic carbon) values (-8 to $+1.7$‰) indicate a stronger contribution from metamorphic degassing occurring at depth along major structural zones such as the MBT, MCT, and ITSZ in the northwest Himalaya [16, 41, 58]. This could be a reason behind low occurrence of calcite and aragonite as hydrothermally altered mineral in Changlung while thermal waters are highly enriched with fluoride (10–12.5 mg/l). The set of equilibrium reactions that are taking place at subsurface of Changlung may be written as follows:

Reaction 1: Fluorite dissolution: $CaF_2 \rightleftharpoons Ca^{2+} + 2F^-$
Reaction 2: Calcite precipitation at subsurface: $Ca^{2+} + 2HCO_3^- \rightleftharpoons CaCO_3 \downarrow + CO_2 \uparrow + H_2O$
Reaction 3: Segregated-CO_2 reabsorption in thermal waters at shallow level: $H_2O + CO_2 \rightleftharpoons H_2CO_3$
Reaction 4: Carbonic acid dissociation near surface: $H_2CO_3 \rightleftharpoons H^+ + HCO_3^-$

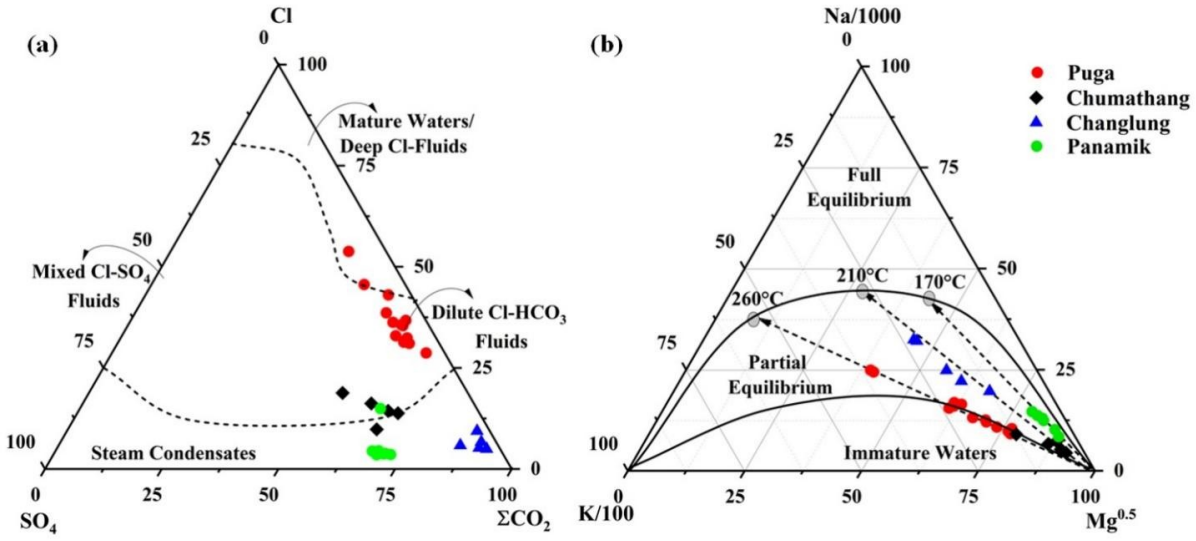

Figure 4. (**a**) Cl–SO_4–$\sum CO_2$ ternary diagram showing water-type to be used for chemical geothermometry; (**b**) Na–K–Mg ternary diagram representing type of equilibration in thermal waters.

All these set of geochemical reactions suggest abnormally high $\sum CO_2$ (1574–1821 mg/l) in thermal waters of Changlung. However, unlike Changlung, Panamik has moderate $\sum CO_2$ concentration, ranging between 258–321 mg/l. In Panamik, the thermal fluids undergo boiling closer to the surface rather than at deeper levels. This near-surface boiling promotes CO_2 degassing and steam segregation, which in turn influences the solubility of calcite and aragonite. As a result, the conditions become favourable for the precipitation of these minerals at the surface. Powder X-ray diffraction analyses of hot-spring deposits from Panamik support this interpretation, showing relatively high calcite contents (∼50% relative intensity ratio (RIR)). In contrast, deposits from Changlung exhibit lower calcite proportions, with RIR values ranging from 20–30% [41]. Most of the hydrothermal minerals present in Changlung in major quantities are trona ($Na_2CO_3{\cdot}NaHCO_3{\cdot}2H_2O$), nahcolite ($NaHCO_3$) and quartz while for Panamik, the predominant minerals in hot spring deposits are quartz and calcite.

5.2. Chemical Geothermometry

To rationally use any geothermal water in chemical geothermometry, the most important criterion to be kept in mind is the equilibration nature of thermal waters, i.e., fully equilibrated, partially equilibrated, or immature, as per Na–K–Mg diagram [1]. In the present study, all the thermal waters are found to be partially equilibrated, however, they show a clustering near Mg-vertex which indicates mixing of thermal waters with non-thermal waters (Figure 4b). However, as thermal waters are partly equilibrated in nature, ion exchange geothermometers can be applied in corroboration with end-members mixing modeling. According to the Na–K–Mg ternary diagram, the reservoir temperatures of thermal waters in the Ladakh Himalaya range from 170 °C to 260 °C, with the higher temperatures characteristic of the Indus River valley systems and the lower temperatures associated with the Shyok–Nubra River valley springs. In this study, Na–K Giggenbach's geothermometer has been used to compute deep fluid composition under partial equilibrium degassing for individual geothermal fields.

5.3. Reservoir Fluid Reconstruction

For Indian geothermal systems, it is reasonable to consider the aquifers as single-phase, liquid-dominated reservoirs because they generally exhibit moderate to low enthalpy. This contrasts with high-temperature geothermal fields such as Krafla and Hellisheidi in Iceland, Olkaria and Paka in Kenya, and Ahuachapán in El Salvador, where steam pockets/caps may coexist with the liquid phase at deeper subsurface levels [59, 60]. When there is a two-phase aquifer, intense boiling may initiate in the high permeable zones due to decompression or addition of excess heat from rock, causing the producing wells to be excess enthalpic where discharge enthalpy may approach enthalpy of pure saturated steam (∼2780 kJ/kg) [2, 19, 61]. The reservoir fluid composition has been reconstructed by adding up the compositions of steam and liquid phases of surface discharge into a single-liquid phase reservoir fluid. The geothermal reservoir water (grw) composition is thereby estimated at reservoir temperature obtained from Na–K Giggenbach's geothermometer. The model used in the present study is proposed by Arnórsson et al. (2007, 2010) where taking into consideration of mass and energy, and using thermodynamic variable enthalpy, adiabatic decompression boiling is carried out in geochemical modeling from the arbitrary temperature of 300 °C to the boiling point of water (100 °C) under partial equilibrium degassing with degassing coefficient, ξ = 0.5, which furnishes us with the boiled reservoir water composition (brw) [2, 62]. For Icelandic geothermal systems, the degree of degassing is commonly assumed to be 30% of equilibrium degassing [63, 64]. Using integrated O, H, Sr isotopic systematics, a binary mixing model between the end-members (magmatic water and snow-melt water) had been proposed for Tibetan geothermal waters like Yangbajing which revealed that the resultant geothermal fluid is a mixture of 40–50% of deep fluid component [21]. Geothermal discharges at Xihai are strongly diluted by non-thermal waters (∼59.5–85.6%), with mixing increasing along the upward flow path and away from major faults, producing a masking or *cover-effect* that must be considered in fault-controlled geothermal fields [22]. The adiabatic boiling modeling, in our study, is carried out in six sequential steps with temperature differences between two consecutive steam-loss processes of 40 °C, rather than a single-flash, and fluid-composition at individual steps have been obtained. The Table 1 describes geothermal reservoir water and boiled reservoir fluid compositions which are used in the subsequent studies as one of the end members to rationalize mixing in thermal waters.

5.4. End-Member Fluid Composition

The formation mechanism of surface geothermal waters is interpreted using three key end-member compositions in a ternary mixing model: non-thermal water (ntw), boiled reservoir water (brw), and condensed steam (cs). A representative average composition of non-thermal waters from the Ladakh Himalayas (N = 6) is used as one vertex in the ternary mixing diagram. The 'cs' end-member is defined using compositions calculated from boiled reservoir water, rather than direct steam-vent samples, to avoid complications arising from steam segregation and condensation that can modify the chemistry of vent-derived steam (Figure 5). The composition of cs is it contains only the volatiles (CGs) which segregated from steam after deep degassing from the residual boiled geothermal fluid, and hence the composition of all non-volatiles in cs is taken to be zero at 100 °C. The end-member composition is shown in Table 1.

Table 1. Compositions of deep reservoir fluid (computed from Na–K Giggenbach's geothermometer) assuming single-phase liquid dominated reservoir and boiled reservoir fluid under partial equilibrium degassing (ξ = 0.5) at 100 °C of different types of geothermal waters from Trans-Himalayas, India. Values are reported in mg/l.

Locations	Puga		Chumathang		Changlung		Panamik			
	Geothermal Reservoir Water	Boiled Reservoir Water (ξ = 0.5)	Geothermal Reservoir Water	Boiled Reservoir Water (ξ = 0.5)	Geothermal Reservoir Water	Boiled Reservoir Water (ξ = 0.5)	Geothermal Reservoir Water	Boiled Reservoir Water (ξ = 0.5)	Representative Non-thermal Water	Condensed Steam
T^{res} (°C)	260	100	235	100	210	100	170	100	10	100
pH_T	7.03	8.59	6.84	8.69	6.87	8.84	6.47	8.22	8.28	5.31
B	91	123	28	34	17	19	7	8	14	0
SiO_2	138	186	138	167	99	114	91	94	18	0
Na	417	566	244	294	592	678	155	161	9	0
K	58	78	22	27	43	49	6	7	3	0
Mg	6	9	16	19	2	3	1	2	10	0
Ca	11	14	20	24	13	15	15	16	28	0
F	8.9	12.1	6.9	8.4	10	11.5	12.1	12.5	0.2	0
Cl	391	530	104	125	101	116	22	24	20	0
SO_4	70	94	157	190	75	87	103	106	5	0
$\sum CO_2$	2117	540	1099	401	2475	1290	519	255	132	6113
H_2S	65	34			56	109				370
TDS	1811	2456	1200	1449	1816	2083	561	578	180	

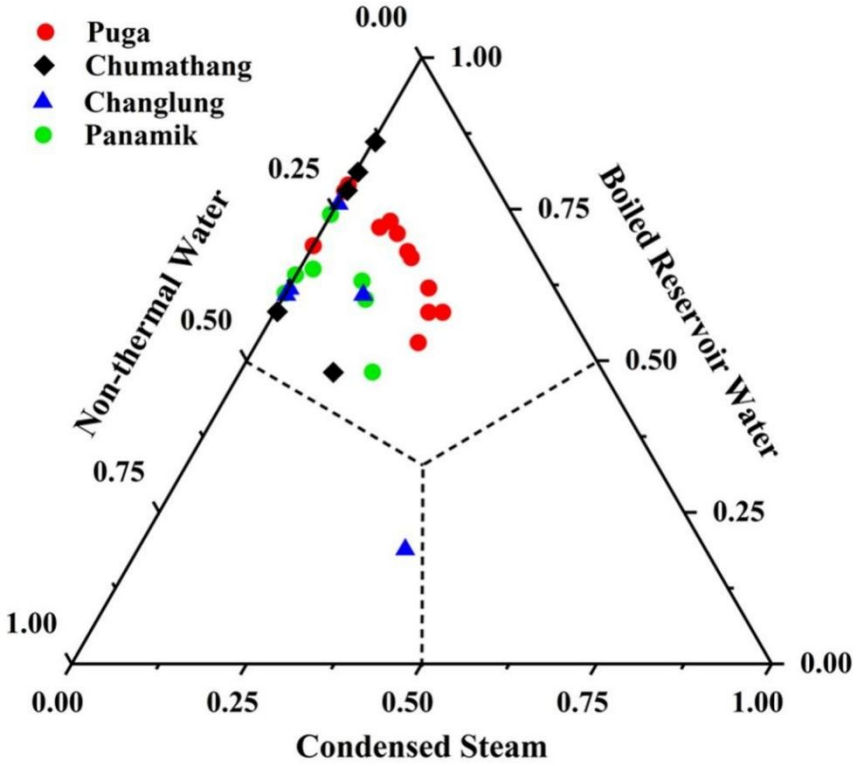

Figure 5. The non-thermal water (ntw), boiled reservoir water (brw), and condensed steam (cs) end-member composition represented in a ternary plot which represents the mixing ratios forming the surface geothermal water in Trans-Himalayan Geothermal Systems, India.

Geothermal fluids are often prone to dilution with non-thermal waters at their outflow zone by a process called mixing which often misleads chemical geothermometers to estimate reservoir temperatures [45, 52]. Mixing processes preferentially occur in zones of abrupt permeability contrasts, especially along the margins of the geothermal reservoir [2, 45]. Such mixing, dilutes the ascending reservoir fluids and alters the activity of reactive chemical species, thereby modifying their saturation indices. These changes can perturb fluid–mineral equilibria and influence the dissolution–precipitation kinetics of various hydrothermal minerals. As Cl is a non-reactive component and always remain in solution due to its higher solubility, it is used as a conservative tracer to quantify the degree of mixing in

thermal fluids of Trans-Himalayas, India [65]. Because enthalpy is conserved during the mixing process, the temperature range of 0–100 °C exhibits a near-linear relationship with enthalpy. This linearity aids the use of components such as SiO_2, Cl, and $\sum CO_2$ to establish correlations with discharge temperature, allowing the compositions of thermal fluids to be quantitatively expressed relative to the contributing end-members.

The end-members mixing model can be represented by the equations as follows:

$$X^{cs} m_{Cl}^{cs} + X^{brw} m_{Cl}^{brw} + X^{ntw} m_{Cl}^{ntw} = m_{Cl}^{m} \quad (4)$$

$$X^{cs} T^{cs} + X^{brw} T^{brw} + X^{ntw} T^{ntw} = T^{m} \quad (5)$$

$$X^{cs} + X^{ntw} + X^{brw} = 1 \quad (6)$$

where 'X', 'm_{Cl}', and 'T' represent the representation for mixing fraction, concentration of Cl (conservative component) in mg/l, and temperature respectively of brw, ntw, and cs. Using Cramer's rule (for a 3 × 3 matrix system with three independent variables), we solve for the results of the mixing model which are given in Table 2. The calculation provides values both negative and higher than unity which have no practical physical significance. Negative mixing fractions values could typically result from conductive cooling, analytical errors in water and gas chemistry. Conversely, fractions exceeding unity usually indicate underestimation of end-member concentrations or enthalpy, or the influence of unaccounted processes such as steam loss or mineral precipitation. Such anomalies generally reflect limitations in end-member selection or deviations from ideal conservative behaviour [20, 45, 66, 67].

Table 2. Results of mixing model between three end-members: boiled reservoir water (brw), condensed steam (cs), and non-thermal water (ntw) for thermal waters of Trans-Himalayas, India.

Sample ID	Location	X^{cs}	X^{brw}	X^{ntw}
PG/1–22	Puga	0.15	0.67	0.18
PG/2–22	Puga	0.20	0.62	0.18
PG/3–22	Puga	0.09	0.73	0.18
PG/4–22	Puga	0.11	0.71	0.18
PG/5–22	Puga	0.14	0.68	0.18
PG/6–22	Puga	0.08	0.72	0.20
PG/7–22	Puga	0.00	0.78	0.22
PG/8–22	Puga	0.24	0.58	0.18
PG/9–22	Puga	0.23	0.53	0.24
PG/10–22	Puga	0.22	0.58	0.20
PG/11–22	Puga	0.00	0.79	0.21
PG/12–22	Puga	0.00	0.78	0.22
PG/13-22	Puga	0.00	0.69	0.31
CH/01–22	Chumathang	0.00	0.78	0.22
CH/02–22	Chumathang	0.00	0.81	0.19
CH/03–22	Chumathang	0.00	0.86	0.14
CH/04–22	Chumathang	0.00	0.58	0.42
CH/05–22	Chumathang	0.13	0.48	0.39
CHL-01	Changlung	0.11	0.61	0.28
CHL-02	Changlung	0.00	0.76	0.24
CHL-03	Changlung	0.00	0.62	0.38
CHL-04	Changlung	0.00	0.61	0.39
CHL-05	Changlung	0.38	0.43	0.19
PNK-01	Panamik	0.00	0.74	0.26
PNK-02	Panamik	0.10	0.63	0.27
PNK-03	Panamik	0.00	0.64	0.36
PNK-04	Panamik	0.12	0.60	0.28
PNK-05	Panamik	0.02	0.65	0.33
PNK-06	Panamik	0.00	0.61	0.39
PNK-07	Panamik	0.19	0.48	0.33

Foot notes: (a) The negative values are meaningless; hence, they are taken to be zero. (b) The values greater than one is taken to be unity. Calculations done after [20]. (c) Values recalculated assuming that the summed fractions of condensed steam, boiled reservoir water, and non-thermal water in the resultant thermal discharge equal unity.

The surface discharge fluid of Puga is a resultant mixture of condensed steam whose proportion during sampling is X^{cs} = 0.08–0.24 (8–24%), with major contributions from boiled reservoir fluids (X^{brw}= 0.53–0.79 (i.e., 53–79%), mean ∼0.68, i.e., 68%) and minor from non-thermal water (X^{ntw}= 0.18–0.31 (i.e., 18–31%), mean ∼0.20, i.e., 20%). Similar trend is also observed for Chumathang fluids where boiled reservoir fluids contribute 48–86% with average value of 70% and non-thermal water of 14–42% with average value of 27%. The average contribution of condensed steam in resultant surface fluid mixture is 13%. The Changlung and Panamik fluids are comprised of 43–76% and 48–74% of boiled reservoir water, 11–38% and 2–19% of condensed steam, and 19–39% and 26–39% of non-thermal water, respectively. Shallow reabsorption of CO_2 in Changlung after steam segregation from deeper levels enhances the concentration of HCO_3 in thermal waters. This process may alter the apparent Cl contribution used in end-member estimations, effectively masking or nullifying the inferred inputs from boiled deep reservoir water and condensed steam. For Panamik, as the fluids are boiling at very shallow level, contributions from three end-members are conspicuous. Recent studies suggest that probably, the thermal waters of Changlung are mixed with local non-thermal waters, following the regional hydraulic gradient, in the outflow zone to emerge as Panamik thermal springs [15, 41, 68, 69].

5.5. Boiling and Degassing

The decompression boiling process influences thermal fluid composition from reservoir to surface with varying proportions of steam-to-liquid ratio, pH, volatiles loss, isotopic fractionation, oxidation, redox behaviour, and fluid-mineral equilibrium reactions [2, 7, 19]. During pressure-induced boiling, most non-condensable gases and a large fraction of condensable gases partition into the steam phase, while the remaining liquid becomes progressively enriched in non-volatile components. The amounts of condensable gases retained in the residual fluid is controlled by their distribution coefficients and the prevailing temperature.

In this study, both the non-conservative (SiO_2 and $\sum CO_2$) and conservative components (Cl) of non-thermal and thermal waters are plotted with the discharge temperatures for all the geothermal fields (Figure 6). The end-members are also plotted in the same diagram to understand the mixing fractions which finally gives the fluid composition similar to the surface discharge. The depressurization boiling process from an isolated system (a thermodynamic system that cannot exchange matter and energy) causes cooling in the shallow reservoir which is further enhanced through mixing with non-thermal waters in the zone of anisotropic permeability [45]. This process influences solubilities of various components leading to supersaturation (precipitation) or undersaturation (dissolution) of pre-equilibrated minerals with the reservoir, in the hydrothermal vents, which in turn seals the fluid flow channels in long-run, a phenomenon called scaling in geothermal project development management.

For SiO_2 vs. temperature relationship plot, silica contents from both surface discharges and boiled reservoir water at 100 °C under partial-equilibrium degassing are plotted with quartz solubility curves drawn for maximum steam loss, no steam loss, and amorphous silica solubility line. None of the data of thermal waters from any geothermal fields touch the amorphous silica equilibrium curve, suggesting that, at surface, thermal waters are undersaturated with amorphous silica but may be in equilibrium or supersaturated with chalcedony or quartz. However, inspite of supersaturation of thermal waters with quartz, in practical, only chalcedony silica scaling may be observed due to sluggish precipitation kinetics of quartz than other kinetic polymorphs of silica for Trans-Himalayan geothermal fluids. The boiling trend lines are shown from the respective boiled reservoir water composition at 100 °C to surface discharge (Figure 6a). The greater extent of water-rock interaction trend line is also shown from non-thermal water to Panamik to Puga, pointing towards more matured and equilibrated reservoir waters from Panamik to Puga.

Negligible effect of boiling on chloride content is observed in chloride vs. temperature relationship plot for thermal waters of Trans-Himalayas suggesting its predominant enrichment in liquid phase after steam segregation during depressurization boiling (Figure 6b). However, all thermal waters are diluted with varying extent of relative boiled reservoir fluid content. Geochemical modeling indicates that surface-discharge thermal fluids of all sites have boiled water fraction greater than 50% with few samples from Changlung, Panamik and Chumathang have values between 40–50% suggesting dilution with non-thermal water of deep aquifer fluids. In $\sum CO_2$ and temperature plot, Changlung waters display greater contribution from condensed steam end-member (∼11–34%), followed by Puga water which is formed by ∼8–24% (mean value 11%) of condensed steam. The contribution of condensed steam is the lowest in Chumathang (∼13% mean value 3%) and Panamik (∼2–19%, mean value 6%) (Figure 6c). For the case of Changlung hot spring, the deeply-degassed CO_2 due to decompression boiling and phase segregation may get reabsorbed by the geothermal fluids at a shallower level to enhance the concentration of HCO_3 ion, thereby also affecting the solubility of calcite [44, 45, 52]. Thus, the highest condensed steam contribution, is likely characterized by shallow and efficient boiling of deep geothermal fluids. However, pH of Changlung fluids is neutral to moderately alkaline probably to the effect of decompression boiling [2, 19, 20, 23]. Thus, the modeling results fit well in corroboration with the end-member mixing composition.

Based on the study, probable hydrogeological settings of the studied geothermal areas can be identified. The hydrogeological setting is primarily controlled by deep-seated faults (Zildat and Kiagar Tso fault-boundaries at Puga, Karakoram fault at Changlung–Panamik) that act as

upflow conduits for thermal fluids, while shallow fracture networks, valley-fill sediments, and river–glacial recharge zones (Indus river for Puga–Chumathang and Nubra river for Changlung–Panamik) facilitate mixing with meteoric groundwater [13–16, 41, 68, 69]. Puga represents a relatively confined upflow system with limited dilution, whereas Changlung and Panamik are characterized by open, shallow circulation and high recharge, leading to stronger meteoric mixing. Chumathang shows an intermediate setting, where thermal fluids interact with shallow aquifers associated with major river systems during their final ascent [7, 18, 49].

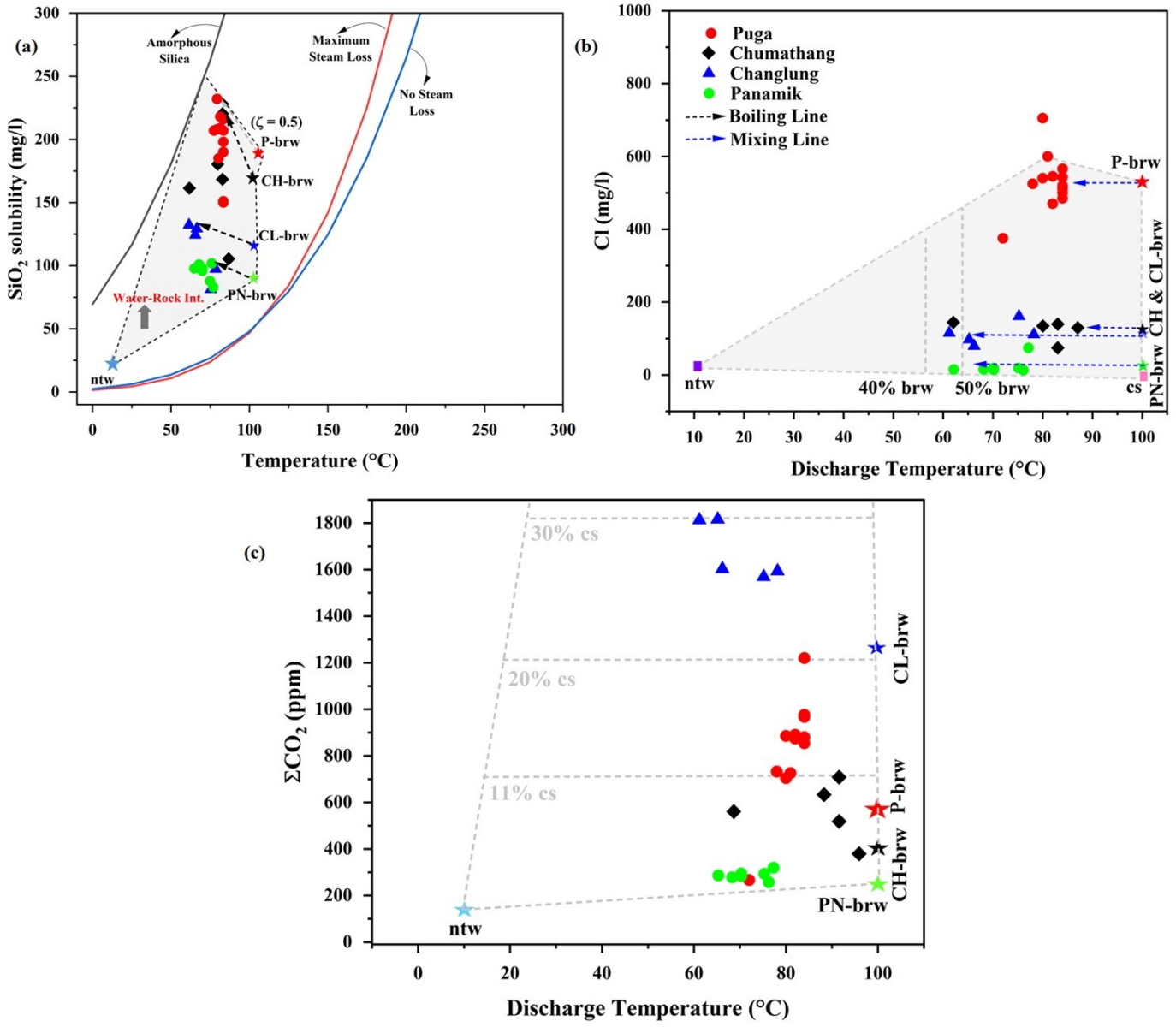

Figure 6. Geochemical evidence of boiling, steam loss, and mixing processes affecting surface thermal waters in the studied geothermal fields. (**a**) Relationship between SiO_2 solubility and temperature showing measured silica concentrations of surface discharges and reconstructed boiled reservoir waters plotted against quartz solubility curves for no steam loss, maximum steam loss, and amorphous silica. The data indicate partial equilibrium degassing and undersaturation with respect to amorphous silica, reflecting boiling and water–rock interaction during ascent. (**b**) Variation of Cl concentration with discharge temperature illustrating conservative behaviour of Cl during boiling and progressive dilution along mixing lines between boiled reservoir water (brw) and non-thermal water (ntw), with estimated proportions of boiled reservoir water. (**c**) $\sum CO_2$ and discharge temperature plot highlighting CO_2 loss during boiling and steam separation, followed by shallow mixing. Black dashed lines represent boiling and degassing trajectories, whereas blue dashed lines denote mixing trends. Symbols correspond to different geothermal fields.

6. Conclusions

In this study, various secondary processes of reservoir like mixing, degassing, and boiling are quantified based on end-member fluid composition determination and reconstruction of deep fluid for the geothermal waters of Trans-Himalayas, India. The study reveals that all the hot waters of Trans-Himalayan geothermal province are mixed with non-thermal water, boiled reservoir waters, and condensed steam in various ratios which can be numerically quantified. The pHs of all deep fluids are near neutral at estimated reservoir temperatures from Na–K Giggenbach's geothermometer, and all the fluids compositions are influenced by decompression boiling, as evident from their moderate alkaline nature at 100 °C under partial equilibrium degassing. The reconstructed surface discharge fluids indicate that Puga and Chumathang systems are dominantly controlled by boiled reservoir water, contributing on average ∼68% and ∼70%, respectively, with subordinate inputs from non-thermal water (∼20–27%) and condensed steam (∼8–24%; average ∼13%). In contrast, Changlung and Panamik fluids exhibit more variable mixing proportions, with boiled reservoir water contributing ∼43–76% and ∼48–74%, respectively, accompanied by relatively higher and variable condensed steam (up to ∼38%) and non-thermal water fractions (∼19–39%). Overall, the results highlight a stronger deep-reservoir signature in Puga and Chumathang compared to the more heterogeneous mixing observed in Changlung and Panamik. This approach enables quantitative evaluation of secondary reservoir processes, providing a robust preliminary insight into geothermal reservoir dynamics where isotopic analyses are economically constrained. It also facilitates assessment of groundwater–geothermal fluid interactions influencing thermal water chemistry. Notably, this study presents the first integrated quantitative reconstruction of deep fluids and their evolutionary pathways in an Indian geothermal system, elucidating the key roles of boiling, degassing, and mixing in controlling Trans-Himalayan geothermal fluid chemistry.

Supplementary Materials

The following supporting information can be downloaded at: https://doi.org/10.53941/esrs.2026.100009, Table S1; Table S2.

Author Contributions

A.D.: Investigation, Formal Analysis, Methodology, Validation, Software, Field sampling, Writing-original draft, Conceptualization; S.C.: Formal Analysis, Writing-original draft, Investigation, Validation, Writing—Review & Editing; P.M.: Investigation, Field sampling, Formal Analysis, Methodology; A.S.: Investigation, Field sampling, Formal Analysis, Methodology; A.B.: Supervision, Resources, Project Administration, Writing-original draft, Writing—Review & Editing; M.L.D.: Supervision, Validation, Writing—Review & Editing; P.K.S.: Supervision, Resources, Writing—Review & Editing; B.R.: Supervision, Resources, Writing—Review & Editing; V.P.M.: Supervision, Validation, Writing—Review & Editing. All authors have read and agreed to the published version of the manuscript.

Funding

This research received no external funding.

Institutional Review Board Statement

Not applicable.

Informed Consent Statement

Not applicable.

Data Availability Statement

All the data utilized in this study are fully presented within the paper.

Acknowledgments

We sincerely express our gratitude to M. Santosh, Earth Systems, Resources, and Sustainability (ESRS) Journal, for kindly inviting us to contribute to the thematic issue on Geothermal Systems in the Himalayas. It is a distinct privilege to be associated with the inaugural volumes of this promising journal. A.D., P.M.. A.S., and A.B. acknowledge Additional Director General and Head of Department, Geological Survey of India, Northern Region, Lucknow and Ministry of Mines, Govt. of India for providing infrastructural, financial, and administrative supports for smooth execution of the field works carried out in the field seasons 2017–18, 2022–23, and 2025–26. S.C. acknowledges R. Acahrya, IRAD, BARC and K. Tirumalesh, Isotope Hydrology Section, IRAD, BARC for their support during the study. We thank Fei Xue and the anonymous reviewers for their insightful comments that improved the quality of the manuscript.

Conflicts of Interest

The authors declare no conflict of interest, and they have no known competing financial interests or personal relationships that could have appeared to influence the work reported in this paper.

Use of AI and AI-assisted Technologies

The authors utilized the Grammarly English correction tool during the preparation of this work. The content was reviewed and edited as necessary by all the authors.

References

1. Giggenbach, W.F. Geothermal solute equilibria. Derivation of Na-K-Mg-Ca geoindicators. *Geochim. Cosmochim. Acta* **1988**, *52*, 2749–2765.
2. Arnórsson, S.; Stefánsson, A.; Bjarnason, J.O. Fluid–fluid interactions in geothermal systems. *Rev. Mineral. Geochem.* **2007**, *65*, 259–312.

3. Balaram, V.; Santosh, M. Critical metal deposits in terrestrial and oceanic environments and the global energy transition. *Habitable Planet* **2025**, *1*, 86–107.
4. Nuñez-Hernández, S.; Pinti, D.L.; López-Hernández, A.; et al. Phase segregation, boiling, and reinjection at the Los Azufres Geothermal Field, Mexico, monitored by water stable isotopes, chloride, and enthalpy. *J. Volcanol. Geotherm. Res.* **2020**, *390*, 106751.
5. Gunnarsson-Robin, J.; Stefánsson, A.; Ono, S.; et al. Sulfur isotopes in Icelandic thermal fluids. *J. Volcanol. Geotherm. Res.* **2017**, *346*, 161–179.
6. Heřmanská, M.; Stefánsson, A.; Scott, S. Supercritical fluids around magmatic intrusions: IDDP-1 at Krafla, Iceland. *Geothermics* **2019**, *78*, 101–110.
7. Dutta, A.; Mishra, P.; Mukherjee, A.; et al. Geochemical evolution of geothermal waters in Trans-Himalayas: Implications for critical mineral deposition. *Geochemistry* **2025**, *85*, 126348.
8. Ricci, A.; Kleine, B.I.; Fiebig, J.; et al. Equilibrium and kinetic controls on molecular hydrogen abundance and hydrogen isotope fractionation in hydrothermal fluids. *Earth Planet. Sci. Lett.* **2022**, *579*, 117338.
9. Chatterjee, S.; Sharma, S.; Ansari, M.A.; et al. Characterization of subsurface processes estimation of reservoir temperature in Tural-Rajwadi geothermal fields, Maharashtra, India. *Geothermics* **2016**, *59*, 77–89.
10. Chatterjee, S.; Mishra, P.; Keesari, T.; et al. Why is it imperative to use multicomponent geothermometry in medium/low enthalpy thermal waters? Insights from the Gujarat geothermal region, India. *Environ. Earth Sci.* **2023**, *82*, 557.
11. Chandrasekharam, D.; Bundschuh, J. *Low-Enthalpy Geothermal Resources for Power Generation*, 1st ed.; CRC Press: Boca Raton, FL, USA, 2007.
12. Sakhare, V.V.; Biswal, B.P.; Rajan, L.C.; et al. *Geothermal Atlas of India*; GSI Special Publ. 125; Geological Survey of India: Kolkata, India, 2022.
13. Mishra, P.; Absar, A.; Dutta, A.; et al. Hot springs of Demchok, Ladakh, India. *Curr. Sci.* **2023**, *124*, 1104–1107.
14. Craig, J.; Absar, A.; Bhat, G.; et al. Hot springs and the geothermal energy potential of Jammu & Kashmir State, NW Himalaya, India. *Earth Sci. Rev.* **2013**, *126*, 156–177.
15. Tiwari, S.K.; Rai, S.K.; Bartarya, S.K.; et al. Stable isotopes ($\delta^{13}C_{DIC}$, δD, $\delta^{18}O$) and geochemical characteristics of geothermal springs of Ladakh and Himachal (India): Evidence for CO_2 discharge in northwest Himalaya. *Geothermics* **2016**, *64*, 314–330.
16. Dutta, A.; Mishra, P.; Absar, A.; et al. Tracing hydrothermal mineral thenardite in geysers/hot springs of North-western Himalayan belt, Ladakh Geothermal Province, India by hydrogeochemistry, fluid-mineral equilibria and isotopic studies. *Geochemistry* **2023**, *83*, 125973.
17. Clark, D.E.; Galeczka, I.M.; Gíslason, S.R.; et al. Does the release of toxic metals due to subsurface CO_2 storage in basalts pose an environmental hazard? *Int. J. Greenh. Gas Control* **2026**, *149*, 104526.
18. Shanker, R.; Absar, A.; Srivastava, G.C.; et al. A case study of Puga geothermal system, India. In Proceedings of the 22nd NZ Geothermal Workshop, Auckland, New Zealand, 2000. ISBN: 0-86869-024-4.
19. Scott, S.; Gunnarsson, I.; Arnórsson, S.; et al. Gas chemistry, boiling and phase segregation in a geothermal system, Hellisheidi, Iceland. *Geochim. Cosmochim. Acta* **2014**, *124*, 170–189.
20. Stefánsson, A.; Keller, N.S.; Robin, J.G.; et al. Quantifying mixing, boiling, degassing, oxidation and reactivity of thermal waters at Vonarskard, Iceland. *J. Volcanol. Geotherm. Res.* **2016**, *309*, 53–62.
21. Guo, Q.; Wang, Y.; Liu, W. O, H, and Sr isotope evidences of mixing processes in two geothermal fluid reservoirs at Yangbajing, Tibet, China. *Environ. Earth Sci.* **2010**, *59*, 1589–1597.
22. Zhang, Y.; Xiao, Y.; Yang, H.; et al. Hydrogeochemical and isotopic insights into the genesis and mixing behaviors of geothermal water in a faults-controlled geothermal field on Tibetan Plateau. *J. Clean. Prod.* **2024**, *442*, 140980.
23. Hurwitz, S.; Stefánsson, A.; Shock, E.L.; et al. The geochemistry of continental hydrothermal systems. In *Treatise on Geochemistry*, 3rd ed.; Holland, H.D., Turekian, K.K., Eds.; Elsevier: Amsterdam, The Netherlands, 2024; pp. 301–345.
24. Scott, S.; Driesner, T.; Weis, P. Boiling and condensation of saline geothermal fluids above magmatic intrusions. *Geophys. Res. Lett.* **2017**, *44*, 1696–1705.
25. Searle, M.; Cooper, D.; Rex, A.; et al. Collision tectonics of the Ladakh-Zanskar Himalaya. *Philos. Trans. R. Soc.* **1988**, *326*, 117–150.
26. Thakur, V.C.; Misra, D.K. Tectonic framework of the Indus and Shyok suture zones in Eastern Ladakh, Northwest Himalaya. *Tectonophysics* **1984**, *110*, 77–93.
27. de Sigoyer, J.; Chavagnac, V.; Blichert-Toft, J.; et al. Dating the Indian continental subduction and collisional thickening in the northwest Himalaya: Multichronology of the Tso Morari eclogites. *Geology* **2000**, *28*, 487–490.
28. Guillot, S.; de Sigoyer J.; Lardeaux, J.; et al. Eclogitic metasediments from the Tso Morari area (Ladakh, Himalaya): Evidence for continental subduction during India-Asia convergence. *Contrib. Mineral Petrol.* **1997**, *128*, 197–212.
29. Bhargava, O.N. *The Geology of the Indus Suture Zone in Ladakh, Himalaya*; Geological Survey of India: Calcutta, India, 1995.
30. Honegger, K.; Dietrich, V.; Frank, W.; et al. Magmatism and metamorphism in the Ladakh Himalayas (the Indus-Tsangpo suture zone). *Earth Planet. Sci. Lett.* **1982**, *60*, 253–292.
31. Pedersen, R.B.; Searle, M.T.; Corfield, R.I. U–Pb zircon ages from the Spontang ophiolite, Ladakh Himalaya. *J. Geol. Soc.* **2001**, *158*, 513–520.
32. Reuber, I. The Dras arc: Two successive volcanic events on eroded oceanic crust. *Tectonophysics* **1989**, *161*, 93–106.
33. Mahéo, G.; Bertrand, H.; Guillot, S.; et al. The South Ladakh ophiolites (NW Himalaya, India): An intra-oceanic tholeiitic arc origin with implication for the closure of the Neo-Tethys. *Chem. Geol.* **2004**, *203*, 273–303.
34. Garzanti, E.; Van Haver, T. The Indus Clastics: Forearc basin sedimentation in the Ladakh Himalaya. *Sediment. Geol.* **1988**, *59*, 237–249.
35. Clift, P.D.; Carter, A.; Krol, M.; et al. Constraints of India–Eurasia collision in the Arabian Sea region taken from the Indus Group, Ladakh Himalaya, India. In The Tectonic and Climatic Evolution of the Arabian Sea Region; Clift, P.D., Kroon, D., Gaedicke, C., et al., Eds.; Geol. Soc. Spec. Pub. 195; Geological Society of London: London, UK, 2002; pp. 97–116.
36. Searle, M.; Weinberg, R.F.; Dunlap, W.J. Transpressional tectonics along the Karakoram fault zone, northern Ladakh: Constraints on Tibetan extrusion. *Geol. Soc. Spec. Publ.* **1998**, *135*, 307–326.
37. Ravikant, V.; Wu, F.Y.; Ji, W.Q.; Zircon U-Pb and Hf isotopic constraints on petrogenesis of the Cretaceous-Tertiary granites in eastern Karakoram and Ladakh, India. *Lithos* **2009**, *110*, 153–166.
38. Debon, F.; Ali Khan, N. Alkaline orogenic plutonism in the Karakorum batholith: The Upper Cretaceous Koz Sar complex (Karambar valley, N. Pakistan). *Geodin. Acta* **1996**, *9*, 145–160.
39. Zhang, M.; Xie, X.-G.; Liu, W.; et al. Hydrothermal degassing through the Karakoram fault, western Tibet: Insights into active deformation driven by continental strike-slip faulting. *Geophys. Res. Lett.* **2024**, *51*, e2023GL106647.
40. Geological Map of India. Geological Survey of India, 1998. Available online: www.gsi.gov.in (accessed on 1 December 2025).
41. Mishra, P.; Dutta, A.; Absar, A.; et al. Tracing the evolution of shallow geothermal springs in the Shyok–Nubra Valley of North-West Himalayas, India through hydrogeochemistry and stable isotopes

(δ^{18}O, δD). *Solid Earth Sci.* **2024**, *9*, 100175.

42. Arnórsson, S.; Bjarnason, J.Ö.; Giroud, N.; et al. Sampling and analysis of geothermal fluids. *Geofluids* **2006**, *6*, 203–216.
43. APHA (American Public Health Association, American Water Works Association, and Water Environment Federation). *Standard Methods for the Examination of Water and Wastewater*, 24th ed.; American Public Health Association (APHA): Washington DC, USA, 2023.
44. Ármannsson, H.; Óskarsson, F.; Fridriksson, T. Geochemical exploration techniques. In *Comprehensive Renewable Energy*, 2nd ed.; Elsevier: Oxford, UK, 2022; pp. 80–97.
45. Arnórsson, S. *Isotopic and Chemical Techniques in Geothermal Exploration, Development, and Use*; International Atomic Energy Agency (IAEA): Vienna, Austria, 2000; pp. 66–248.
46. Bjarnason, J.Ö. *The Chemical Speciation Program WATCH*, *version 2.4*; ÍSOR Iceland: Reykjavík, Iceland, 2010.
47. Parkhurst, D.L.; Appelo, C.A.J. *User's Guide to PHREEQC: A Computer Program for Speciation, Batch-Reaction, One-Dimensional Transport, and Inverse Geochemical Calculations (No. 99-4259)*, *Version 2*; US Geological Survey: Reston, VA, USA, 1999.
48. Giggenbach, W.F. Graphical techniques for the evaluation of water/rock equilibration conditions by use of Na, K, Mg and Ca contents of discharge waters. In Proceedings of the 8th New Zealand Geothermal Workshop, Auckland, New Zealand, 21–23 January 1986, pp. 37–44.
49. Tiwari, S.K.; Yadav, J.S.; Sain, K.; et al. Impact of geothermal activity on the anomalous retreat of Changmolung Glacier in the Karakoram. *Sci. Tot. Environ.* **2025**, *999*, 180332.
50. Jeelani, G.; Lone, S. A.; Deshpande, R. D.; et al. Origin and evolution of fluids and heatflow in geothermal systems of Indus River Basin (IRB), India. *Sci. Rep.* **2025**, *15,* 43746.
51. Kumar, P.V.; Patro, P.K.; Azeez, K.A.; et al. Inferred secondary magma pathways between Puga and Chumathang geothermal systems from magnetotelluric data in the Himalayan collisional zone. *Earth Planets Space* **2026**, *78,* 3.
52. Nicholson, K. *Geothermal Fluids Chemistry and Exploration Techniques*, 1st ed.; Springer-Verlag: Berlin, Heidelberg, Germany, 1993.
53. Dutta, A.; Mishra, P.; Thapliyal, A.P.; et al. Implication of epithermal mineralization as proxy for geothermal energy potentiality in Puga, Ladakh UT, India. *Earth Sci.* **2024**, *13*, 8–13.
54. Ansari, A.H.; Das, A.; Ansari, N.G.; et al. *T*racing early life on Mars: Lessons from organics produced in high-altitude hot springs of Ladakh. *Prog. Earth Planet. Sci.* **2025**, *12*, 1–19.
55. Sarkar, S.; Moitra, H.; Bhattacharya, S.; et al. 2022. Spectroscopic studies on the Puga Hot Spring Deposits, Ladakh, an astrobiological Martian analog site in India. *J. Geophys. Res. Planets* **2022**, *127*, e2022JE007299.
56. Phartiyal, B.; Kumar, A.; Shukla, S. Martian/Lunar analogue research station in India: Ladakh as a potential site. *Curr. Sci.* **2025**, *128*, 00113891.
57. Chaddha, A.S.; Shukla, S.K.; Sharma, A.; et al. Calcium carbonate as a potential template for the origin of life: Coupled inorganic–organic geochemistry of travertine deposit from Puga hot spring. *ACS Earth Space Chem.* **2025**, *9*, 1905–1926.
58. Mishra, P.; Dutta, A.; Malviya, V.P.; et al. Conceptual modelling on water-rock reaction and genesis of high pH fluids in a typical granitoid geothermal reservoir: A case from Indus-Tsangpo Suture Zone, India. *Phys. Chem. Earth Parts A/B/C* **2024**, *136*, 103736.
59. Axelsson, G.; Arnaldsson, A.; Ármannsson, H.; et al. Updated conceptual model and capacity estimates for the Greater Olkaria geothermal system, Kenya. In Proceedings of the Thirty-Eighth Workshop on Geothermal Reservoir Engineering, Stanford, CA, USA, 11–13 February 2013.
60. Ciriaco, A.E.; Zarrouk, S.J.; Zakeri, G. Geothermal resource and reserve assessment methodology: Overview, analysis and future directions. *Renew. Sustain. Energy Rev.* **2020**, *119*, 109515.
61. Stefánsson, A.; Barnes, J.D. Chlorine isotope geochemistry of Icelandic thermal fluids: Implications for geothermal system behavior at divergent plate boundaries. *Earth Planet. Sci. Lett.* **2016**, *449*, 69–78.
62. Arnórsson, S.; Angcoy, E.; Bjarnason, J.Ö.; et al. Gas chemistry of volcanic geothermal systems. In Proceedings of the World Geothermal Congress, Bali, Indonesia, 25–30 April 2010.
63. Gunnarsson, I.; Arnórsson, S. Amorphous silica solubility and the thermodynamic properties of H_4SiO_4 in the range of 0 to 350°C at P_{sat}. *Geochim. Cosmochim. Acta* **2000**, *64*, 2295–2307.
64. Stefánsson, A.; Arnórsson, S. Feldspar saturation state in natural waters. *Geochim. Cosmochim. Acta* **2000**, *64*, 2567–2584.
65. Arnórsson, S.; Andrésdóttir, A. Processes controlling the distribution of boron and chlorine in natural waters in Iceland. *Geochim. Cosmochim. Acta* **1995**, *59*, 4125–4146.
66. Tole, M.P.; Ármannsson, H.; Zhong-He, P.; et al. Fluid/mineral equilibrium calculations for geothermal fluids and chemical geothermometry. *Geothermics* **1993**, *22*, 17–37.
67. Lelli, M.; Kretzschmar, T.G.; Cabassi, J.; et al. Fluid geochemistry of the Los Humeros geothermal field (LHGF-Puebla, Mexico): New constraints for the conceptual model. *Geothermics* **2021**, *90*, 101983.
68. Patro, P.K.; Dhamodharan, S.; Durga, V.; et al. Delineation of a geothermal source beneath the Panamik-Changlung Hot Springs along the Karakoram Fault, Ladakh, India, using magnetotelluric studies. *J. Volcanol. Geotherm. Res.* **2025**, *468*, 108478.
69. Kumar, D.; Ojha, A.K.; Maurya, V.P.; et al. New insight into the shallow sub-surface for geothermal prospection of Puga valley, Ladakh, India from electrical resistivity tomography. *Geothermics* **2025**, *131*, 103409.